Imitation Learning of Nonlinear Model Predictive Control for Emergency Collision Avoidance

Seungtaek Kim, Kyoungseok Han, *Member, IEEE*, and Seibum B. Choi, *Member, IEEE*

***Abstract*—This study proposes a control structure based on imitation learning (IL) of nonlinear model predictive control (NMPC) for vehicle collision avoidance systems. An NMPC was employed to achieve maximum collision avoidance ability by integrated steering and braking, then later imitated by a deep neural network (DNN) to satisfy real-time capability. Previous studies that imitate NMPC have proven its control performance and computation efficiency. However, there were limitations in applying to vehicle collision avoidance systems. Despite its dangerous situation, data set for imitation should be obtained by experiments using the controlled plant, and weaknesses in handling model parameters were shown. Therefore, this paper proposes a novel IL-based control structure suitable for collision avoidance systems that overcame such limitations by building a feedforward feedback structure so that the data set trained for imitation can be made offline and applying an input dimensionalization process to ensure robustness to parameter changes. CarSim-based human-vehicle interactive simulation experiments demonstrated that the proposed IL-based control structure had no issue applying the offline trained DNN in the simulation while showing robustness to parameter changes.**

***Index Terms*—Imitation learning, Collision avoidance control, Nonlinear model predictive control, Advanced driving assistance systems**

I. Introduction

With the active development of automotive technology across industries, the demand for advanced safety systems has increased in the past three decades [1]. Besides the development of self-driving vehicles, various attempts have been made to develop advanced driving assistance systems (ADASs) that can maximize the possibility of avoiding vehicle crash accidents by taking over the control inputs of the vehicle from human drivers [2]. Such ADASs can compensate for human factors such as misjudgments and slow response by providing precise perception, safe decision algorithms, and advanced control methods [3].

Likewise, collision avoidance systems that can evade the vehicle from accidents with surrounding vehicles [4], [5] and pedestrians [6]–[8] have been in trend to be applied in mass production vehicles by manufacturers. It is well-known that evasive maneuvers based on both steering and braking can maximize the chance of collision avoidance compared to maneuvers involving braking only [9]; therefore, collision avoidance systems with active steering and braking have been studied actively to enhance passenger safety. Both steering and braking should be controlled carefully by considering the complicated nonlinear vehicle dynamics and friction limits for vehicle stability [10]. Many studies attempted to solve these problems via two processes. The first process is to define a collision-free path [11], and the second is to control the vehicle track the path without loss of stability [12].

Studies on collision-free path generations applied techniques such as spline curves [4] or potential fields [5]. Friction limits of the ground were reflected by limiting the curvature, and vehicle ride quality was improved by considering the estimated accelerations. Once the path was generated, studies used various controllers, such as linear quadratic Gaussian control [13], to make the vehicle follow the path. Nonlinear controllers, such as sliding mode control [14] or nonlinear adaptive control [15], were also applied to consider the nonlinearity in positional relations of the vehicle. The above controllers showed great tracking results; however, as the controller demanded the vehicle to behave more urgently, unstable behavior in the vehicle was likely to arise, as the friction limits became violated [4].

On the other hand, model predictive control (MPC) can consider the physical constraints of the friction limits guaranteeing the stability of the controlled vehicle [12]. MPC takes the future reference path into account and calculates the optimal control input satisfying the physical constraints, and therefore is regarded as a suitable path tracker among many types of controllers. Moreover, in the case of the nonlinear MPC (NMPC), nonlinearity in the positional relations of the vehicle can be considered and optimized, as well as the control inputs. This means that the evasive path for collision avoidance can also be optimized using NMPC, where nonlinear vehicle dynamics and physical constraints are considered directly [16], [17]. MPC can be divided into linear MPC (LMPC) and NMPC depending on the model structure that is used [18].

LMPC uses a linear model to formulate convex problems that can be solved with a small amount of computation. Linear vehicle and tire models were used to make the vehicle follow the evasive path. Considering friction limits, linear constraints containing vehicle states, such as slip angles [5] and yaw rate [4], [19], were applied to obtain both tracking performance and vehicle stability. However, tracking controllers using LMPC have limitations in that the accuracy of the linear model becomes poor under extreme situations where nonlinear behaviors of the vehicle become dominant. Therefore, studies often restrict the vehicle behavior in a linear region by controlling the vehicle only by steering [5] or limiting the reference [20] to maintain the model linearity. Using the linearized

Seungtaek Kim and Seibum B. Choi (Corresponding Author) are with the Korea Advanced Institute of Science and Technology, Daejeon 34141, South Korea (e-mail: kimst9o9@kaist.ac.kr and sbchoi@kaist.ac.kr)

Kyoungseok Han (Co-corresponding Author) is with the School of Mechanical Engineering, Kyungpook National University, Daegu 41566, South Korea (e-mail: kyoungsh@knu.ac.kr)

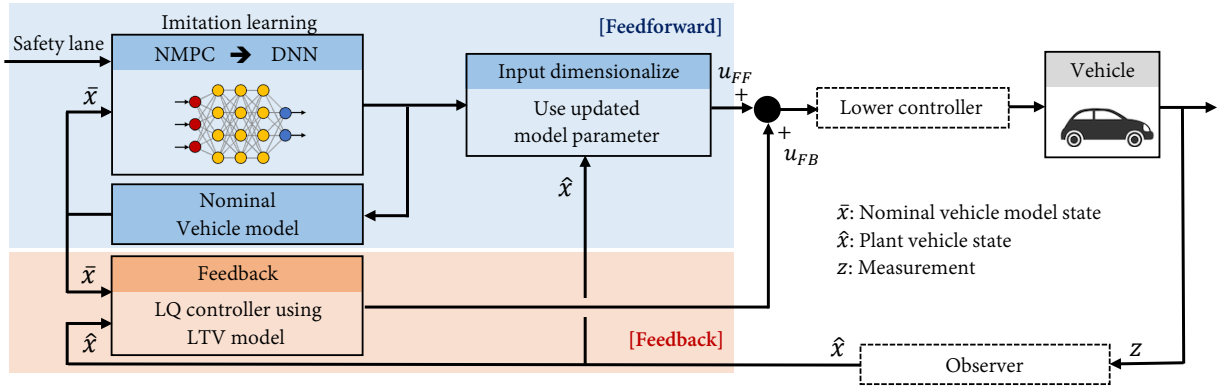

Fig. 1. Proposed control architecture where nonlinear model predictive control (NMPC) is imitated by a deep neural network (DNN) and linearized time-varying (LTV)-linear quadratic (LQ) control are co-located.

model [21], [22] of the nonlinear model mitigated such issues. Integrated control [21] of both steering and differential braking for collision avoidance became possible, resulting in improved tracking performance. However, when the linearization point changes a lot or is no longer valid, the controller performance becomes poor and the optimization problem can be even infeasible [22], such as in an emergency avoidance situation where an obstacle suddenly appears.

NMPC overcomes the drawbacks of the LMPC by handling nonlinear models and constraints directly. It formulates non-convex problems that are solved with a massive computation but guarantee high control performance [18]. Studies considered a nonlinear full-car model with a nonlinear tire model to fully use the behavior of the vehicle under extreme evasive situations [23]. Friction limit circles [24] of each tire were directly handled as nonlinear constraints in the NMPC, guaranteeing more stability in the vehicle behavior. Furthermore, unlike LMPC, in which collision-free paths should be predefined, a path generation process is not required because the avoidance trajectory can also be optimized by considering the nonlinearities related to vehicle position. By only considering the safety lane, the evasive path and the control inputs can be both optimized by the NMPC, showing greater evasive performance than other controllers [16], [17]. However, the high computation load makes its real-time implementation nearly impossible. Therefore, attempts were made to reduce the computation load of NMPC while maintaining its control performance. An attractive method studied recently is applying imitation learning [25] to replace the NMPC with an artificial neural network.

Imitation learning (IL) is derived from reinforcement learning and has been studied for environments where defining an appropriate reward function was difficult. Instead of setting the reward function, IL makes the agent learn directly from the expert's demonstrations. The simplest structure is behavioral cloning [26], famous for applying it to an autonomous vehicle in 1988 [27]. Distributional shift problems existed in behavior cloning, which put the agent into a state that the expert has never visited. Dataset aggregation (DAgger) [28] mitigated such problems by aggregating more training data via the expert's feedback when the agent gets lost. Inverse reinforcement learning [29], famous for generative adversarial imitation learning (GAIL) [30], is another structure for IL that tries to learn the reward function from a limited set of expert demonstrations. While accessibility to experts was a challenge for IL, studies have been actively conducted to imitate NMPC via IL because such problems could be overcome by having NMPC as an expert.

A. Exisiting methods of IL of MPC

One study proposed a guided policy search (GPS) algorithm for a quadrupedal robot. This policy, which is structured in a mixture-of-experts network, is guided by solutions of the NMPC [31]. Control Hamiltonian was proposed as the loss function to improve the constraint satisfaction of the trained policy. A similar NMPC-based GPS approach was used to train a neural network policy for autonomous aerial vehicles, and it achieved successful control without knowledge of the full state [32]. A deep neural network (DNN) was trained using the data buffer obtained from the results of NMPC, and simulation results of applying the DNN to the four-wheel mobile robot were obtained [33]. In the case of vehicle control, an NMPC-based path-tracking controller was trained to a DNN, and NMPC-based and DNN-based controls were compared experimentally; only a slight difference was found between the tracking results [34]. Real-time drifting control of an RC car could be performed by the same method because the nonlinearities of the dynamics were considered [35].

Implementing the IL with NMPC as an expert has been studied actively, and its performance was proven. However, applying it to vehicle avoidance collision control is still challenging for the following reasons. First, data set for imitation is nearly impossible to be obtained from vehicle experiments under collision avoidance situations. However, [33]–[35] require extensive real-world experiments to obtain training data for the DNN, as DNN relies on the plant's current state for control input calculation. Moreover, studies [31], [32] rely on on-policy learning, meaning the policy should be applied during the collision avoidance experiment, which may be very dangerous. Lastly, previous approaches cannot handle parameter changes of the plant because the controller is formed into a single neural network. Dangerous situations can arise if

the safety constraints are not guaranteed to be satisfied under such parameter variation, as vehicles frequently undergo such variations.

B. Proposed method

Therefore, this study proposes a novel control structure based on the IL of the NMPC, which is made suitable for vehicle collision avoidance systems. A DNN is used for imitiating the NMPC. Compared to previous studies, data for training the DNN can be obtained offline using a nominal vehicle model-based simulation, meaning that countless experiments involving the plant vehicle become unnecessary. Robustness to changes in the vehicle parameters was achieved by input dimensionalization, in which the changed parameters were considered and used to modify the control inputs to satisfy the safety constraints under parameter changes.

In case of the NMPC, which is the reference for the DNN, it comprises a nonlinear full-car model and brush tire model representing the complex vehicle dynamics; a cost function that makes the vehicle avoid the collision; and physical constraints based on the friction limits to guarantee vehicle stability. The controller controls the steering angle, and each tire braking forces to make the vehicle move into the safety lane, thereby minimizing the avoiding area to maximize passengers' safety from the pop up obstacles.

The overall control structure is shown in Fig 1. Control inputs are divided into feedforward and feedback. The DNN is applied in the feedforward that makes the nominal vehicle model avoid the collision. This nominal vehicle model is the model used in the NMPC and not the plant vehicle itself. The remaining feedback controller is calculated in real-time, thereby regulating the error between the plant vehicle and the nominal vehicle model. Input dimensionalization modifies the DNN outputs considering the changed vehicle parameters.

C. Contributions

The main contributions of this study are as follows: A suitable control structure based on IL of NMPC for collision avoidance is proposed. (1) This control structure can be trained by offline-made data. (2) It is robust to parameter changes. (3) A novel collision avoidance control for vehicles using IL is proposed, and this control provides excellent evasion performance and real-time control capability.

D. Paper structure

The remainder of this paper is organized as follows. In section II, the NMPC, which is imitated by a DNN, is explained in detail, and the process of IL is introduced. Section III explains the input dimensionalization process, which modifies the control input suitable to the plant vehicle to achieve robustness to parameter changes. Section IV explains the feedback controller. An analysis of experimental verifications via CarSim-based human-vehicle interactive simulation is presented in section V. Finally, the conclusions and future work are mentioned in section VI.

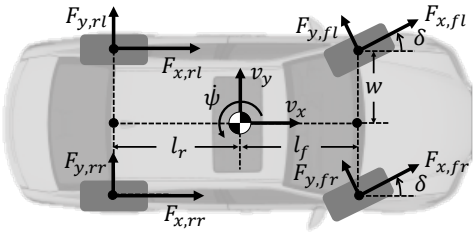

Fig. 2. Nonlinear full-car model.

II. Imitation Learning

This section introduces the components of the IL, namely, NMPC and behavioral cloning.

A. Problem statement

The main objective of the controller is to avoid collision of the vehicle with a pop up obstacle when sufficient space is not available to avoid the crash by braking only. When the collision avoidance system is initiated, the controller controls the braking force of each wheel and the steering angle to maximize the chance of avoiding a collision.

In this study, the priority of the controller is to minimize the avoiding area, allowing more space between the vehicle and obstacle. This approach can maximize the chance of guaranteeing safety to the driver and the passing obstacle. Therefore, the controller tries its best to maneuver the vehicle to the safety lane, regardless of the size or shape of the obstacle. As the NMPC can optimize the evasive trajectory as well, only the safety lane is set as the reference for the controller.

B. Nonlinear model predictive control

In this study, an NMPC was designed to control the vehicle to maneuver it into the safety lane by controlling the steering angle and brake forces. To fully use the vehicle's evasive ability, a nonlinear full-car model with a brush tire model was used for the NMPC prediction model.

1) Nonlinear prediction model: The nonlinear full-car model, shown in Fig. 2, can accurately express the longitudinal, lateral, and yaw movements of the vehicle with reference to the forces on each tire. By applying force-balance and moment-balance equations, the planar motion of the vehicle can be expressed as shown in the following equation [36]:

$$\begin{aligned} ma_x = {} & (F_{x,fl} + F_{x,fr})\cos(\delta) + F_{x,rl} + F_{x,rr} \\ & - (F_{y,fl} + F_{y,fr})\sin(\delta) - C_d v_x^2 \end{aligned} \tag{1a}$$

$$\begin{aligned} ma_y = {} & (F_{y,fl} + F_{y,fr})\cos(\delta) + F_{y,rl} + F_{y,rr} \\ & + (F_{x,fl} + F_{x,fr})\sin(\delta) \end{aligned} \tag{1b}$$

$$\begin{aligned} I_z\ddot{\psi} = {} & l_f\,(F_{y,fl} + F_{y,fr})\cos(\delta) - l_r\,(F_{y,rl} + F_{y,rr}) \\ & + w\,((F_{x,fl} - F_{x,fr})\cos(\delta) + F_{x,rr} - F_{x,rl}) \\ & + l_f\,((F_{x,fl} + F_{x,fr})\sin(\delta)) \\ & + w\,((F_{y,fl} - F_{y,fr})\sin(\delta)) \end{aligned} \tag{1c}$$

where m is the mass of the vehicle; I_z is its moment of inertia; a_x and a_y are the longitudinal and lateral accelerations of

its center of gravity (CG), respectively; v_x is its longitudinal velocity; β is the vehicle slip angle; ψ is the vehicle yaw; δ is the front steering angle; C_d is the air drag coefficient; l_f and l_r are the distances from the vehicle CG to the front and rear axles, respectively; w is the half size of the vehicle width; F_x and F_y are the longitudinal and lateral forces, respectively, acting on each tire. The subscripts fl, fr, rl, and rr represent the front left, front right, rear left, and rear right tires, respectively.

According to the rotational coordinate transformation, a_x and a_y can be expressed as follows:

$$a_x = \dot{v}_x - v_x \beta \dot{\psi} \tag{2a}$$

$$a_y = v_x \left(\dot{\beta} + \dot{\psi} \right) \tag{2b}$$

In addition, the equation for describing the position of the vehicle during the evasion can be expressed as follows:

$$\dot{x}_{\text{pos}} = v_x \cos(\beta + \psi) \tag{3a}$$

$$\dot{y}_{\text{pos}} = v_x \sin(\beta + \psi) \tag{3b}$$

where x_{pos} and y_{pos} is the global longitudinal and lateral positions of the vehicle.

To consider the friction limits of each tire and analyze the tire forces acting on the vehicle, a brush tire model [37] that can handle friction limits and the nonlinear behavior of the tire is applied. As the longitudinal tire forces are the control variables, only the lateral tire forces obtained from the brush tire model are used as follows:

$$F_{y,j} = C_\alpha(\alpha_j, F_{z,j}),\ j = fl, fr, rl, rr$$
$$= \begin{cases} \text{if } |\alpha_j| < \tan^{-1}\left(\frac{3\mu}{C_0}\right) \\ -C_0 F_{z,j} \tan(\alpha_j) + \text{sgn}(\alpha_j) \frac{C_0^2 F_{z,j}}{3\mu} \tan^2(\alpha_j) \\ -\frac{C_0^3 F_{z,j}}{27\mu^2} \tan^3(\alpha_j) \\ \text{otherwise} \\ -\text{sgn}(\alpha_j) \mu F_{z,j} \end{cases} \tag{4}$$

where α is the slip angle of each tire; C_0 is the normalized cornering stiffness at the linear region ($\alpha \ll 1$), μ is the road friction; F_z is the vertical force of each tire.

The slip angle of each tire can be expressed as follows:

$$\alpha_{fl} = \alpha_{fr} = \beta + \frac{l_f}{v_x}\dot{\psi} - \delta \tag{5a}$$

$$\alpha_{rl} = \alpha_{rr} = \beta - \frac{l_r}{v_x}\dot{\psi} \tag{5b}$$

The vertical force of each tire $F_{z,j}$ is calculated considering the effects of shifting of the vehicle weight because of longitudinal/lateral acceleration and roll stiffness of the front and rear axles, as follows [24]:

$$F_{z,fl} = \frac{l_r}{2L} mg - \frac{h_{cg}}{2L} m a_x + \sigma_f m a_y \tag{6a}$$

$$F_{z,fr} = \frac{l_r}{2L} mg - \frac{h_{cg}}{2L} m a_x - \sigma_f m a_y \tag{6b}$$

$$F_{z,rl} = \frac{l_f}{2L} mg + \frac{h_{cg}}{2L} m a_x + \sigma_r m a_y \tag{6c}$$

$$F_{z,rr} = \frac{lf}{2L} mg + \frac{h_{cg}}{2L} m a_x - \sigma_r m a_y \tag{6d}$$

where g is the gravitational acceleration; L is the distance between the front and rear axles; σ_f and σ_r are the front and rear roll stiffness.

Using equations (1)-(6), a nonlinear model that represents the vehicle planar motion can be obtained in a state space form with a state vector and an input vector organized as follows:

$$\dot{x}_v = f_v\left(x_v, u_v\right) \tag{7a}$$

$$x_v = \left[y_{\text{pos}}, \psi, \dot{\psi}, \beta, v_x\right]^T \tag{7b}$$

$$u_v = \left[F_{x,fl}, F_{x,fr}, F_{x,rl}, F_{x,rr}, \delta\right]^T \tag{7c}$$

To fully consider and utilize the evasive capability of a vehicle, the input delays caused by lower controllers should also be considered. Therefore, delays are compensated by augmenting the dynamics of the lower controller in the nonlinear vehicle model [38]. These dynamics are approximated by a first-order linear system as follows:

$$\tau_{F_x} \dot{F}_{x,j} = -F_{x,j} + F_{x,j}^{in},\ j = fl, fr, rl, rr \tag{8a}$$

$$\tau_\delta \dot{\delta} = -\delta + \delta^{in} \tag{8b}$$

where τ_{F_x} and τ_δ are the time constants for the lower controllers, and $F_{x,j}^{in}$ and δ^{in} are the new control variables.

Therefore, by combining (7) and (8), the nonlinear model used for the NMPC is organized as follows:

$$\dot{x} = f(x, u) \tag{9a}$$

$$x = \left[x_v, u_v\right]^T \tag{9b}$$

$$u = \left[F_{x,fl}^{in}, F_{x,fr}^{in}, F_{x,rl}^{in}, F_{x,rr}^{in}, \delta^{in}\right]^T \tag{9c}$$

In addition, to obtain the model in a discrete domain, the nonlinear state space equation is discretized using the fourth-order Runge-Kutta (RK4) and zero-order-hold method as follows:

$$\begin{aligned} x(k+1) &= f_d(x(k), u(k)) \\ &= f_{d,x}(x(k)) + Bu(k) \end{aligned} \tag{10}$$

where $f_d(x(k))$ and B can be expressed as follows using the identity matrix I and $\tau = \text{diag}\left(\tau_{F_x}, \tau_{F_x}, \tau_{F_x}, \tau_{F_x}, \tau_\delta\right)$:

$$f_d(x(k)) = \begin{bmatrix} x_v(k) + \frac{T}{6}(K_1 + 2K_2 + 2K_3 + K_4) \\ e^{-\frac{T}{\tau}} u_v(k) \end{bmatrix} \tag{11a}$$

$$B = \begin{bmatrix} 0 \\ I - e^{-\frac{T}{\tau}} \end{bmatrix} \tag{11b}$$

T is the sampling time, and K_1, K_2, K_3, and K_4 are the components of the RK4 as follows:

$$K_1 = f_v\left(x_{vel}(k), u_v(k)\right) \tag{12a}$$

$$K_2 = f_v\left(x_{vel}(k) + \tfrac{1}{2}K_1 T, u_v(k) + \tfrac{1}{2}\gamma T\right) \tag{12b}$$

$$K_3 = f_v\left(x_{vel}(k) + \tfrac{1}{2}K_2 T, u_v(k) + \tfrac{1}{2}\gamma T\right) \tag{12c}$$

$$K_4 = f_v\left(x_{vel}(k) + K_3 T, u_v(k) + \gamma T\right) \tag{12d}$$

where γ is the $u_v(k)$ rate vector at step k. It can be approximated by calculating the average rate between step k and $k+1$ using (8) as follows:

$$\begin{aligned} \gamma = \frac{du_v(k)}{dt} &\approx \frac{u_v(k+1) - u_v(k)}{T} \\ &= \frac{1 - e^{-\frac{T}{\tau}}}{T}\left(u(k) - u_v(k)\right) \end{aligned} \tag{13}$$

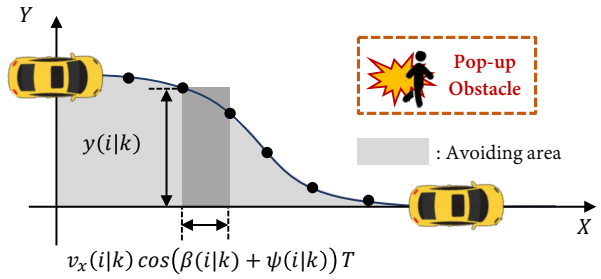

Fig. 3. Calculation of the avoidance area via mensuration by parts. The cost function is defined to minimize the avoidance area required for a vehicle's evasive maneuver.

Using the nonlinear model (10), the future state $X(k)$ of the vehicle is predicted in the NMPC using the following equations:

$$x(i+1|k) = f_d\left(x(i|k), u(i|k)\right),\ i = 0 \sim N-1 \tag{14a}$$

$$U(k) = \left[u(0|k), \cdots, u\left(N-1|k\right)\right]^T \tag{14b}$$

$$X(k) = \left[x(0|k), \cdots, x\left(N|k\right)\right]^T \tag{14c}$$

where $\bullet(i|k)$ is the predicted future value in the $k+i$ step based on the k step; N is the prediction horizon; $X(k)$ is the vehicle's future state; $U(k)$ is the future control input sequence.

2) Cost function: Using the predicted future state of the vehicle, the NMPC optimizes the future control input sequence, minimizing the cost function calculated over the prediction horizon. To maneuver the vehicle immediately into the safety lane in a collision emergency, a cost function regulating the error between the lateral position of the vehicle and the safety lane is defined for the NMPC. The cost function $J(x(0|k), U(k))$ used in the NMPC takes the following form.

$$J(x(0|k), U(k)) = \sum_{i=0}^{N-1} q\left(x(i|k), u(i|k)\right) + p\left(x\left(N|k\right)\right) \tag{15}$$

where $p\left(x\left(N|k\right)\right)$ is the terminal cost, and $q\left(x(i|k), u(i|k)\right)$ is the stage cost.

In this study, the terminal cost is neglected by including a terminal constraint, which will be explained in the next subsection, and the stage cost is organized as follows:

$$\begin{aligned} q\left(x(i|k), u(i|k)\right) &= q_{\text{avoid}}\left(x(i|k), u(i|k)\right) \\ &+ u(i|k)^T R_u u(i|k) \\ &+ \Delta u(i|k)^T R_{\Delta u} \Delta u(i|k) \end{aligned} \tag{16}$$

where $q_{\text{avoid}}\left(x(i|k), u(i|k)\right)$ is the term for regulating the vehicle to the safety lane; R_u and $R_{\Delta u}$ are the positive definite matrices that penalize input, and input change, where input change can be calculated as follows:

$$\Delta u(i|k) = \begin{cases} 0 & \text{if, } i = 0 \\ u(i|k) - u(i-1|k) & \text{else} \end{cases} \tag{17}$$

In previous studies, vehicle was made to track the reference path, which is the safety lane in this study, by penalizing the l_2-norm of the tracking error by defining the stage cost as follows:

$$q_{\text{avoid}}\left(x(i|k), u(i|k)\right) = Q \cdot \left(y_{\text{pos}}(i|k)\right)^2 \tag{18}$$

where Q is the positive gain that penalizes the tracking error. Note that, the safety lane can be always thought as the x-axis without loss of generosity.

The above term has the physical meaning that the tracking error is penalized in the time domain. In the case of a collision avoidance situation, the priority is to ensure the driver's safety during collision; this implies reducing the avoidance area, allowing more space between the vehicle and obstacle. However, maneuvering to the safety lane within a short time does not precisely mean that the vehicle moves to the lane with the smallest avoidance area. Therefore, this study proposes a stage cost penalizing the avoidance area in the space domain rather than in the time domain. The proposed stage cost represents the avoidance area via mensuration by parts, as shown in Fig. 3, summing up the rectangular segments obtained by the left-point rule [39]. Thus, the proposed stage cost can be obtained as follows:

$$\begin{aligned} &q_{\text{avoid}}\left(x(i|k), u(i|k)\right) \\ &= Q_{\text{area}}\left|y_{\text{pos}}(i|k) v_x(i|k) \cos\left(\psi(i|k) + \beta(i|k)\right) T\right| \end{aligned} \tag{19}$$

where Q_{area} is the positive gain that penalizes the avoidance area. By designing such a stage cost, the NMPC makes the vehicle move to the safety lane, thereby minimizing the avoidance area, and ensuring a higher possibility of collision avoidance.

A simple verification was performed to show the difference between two NMPCs with different stage costs; one with the space domain and the other with the time domain. Fig. 4 shows the evasive vehicle trajectory and velocity optimized

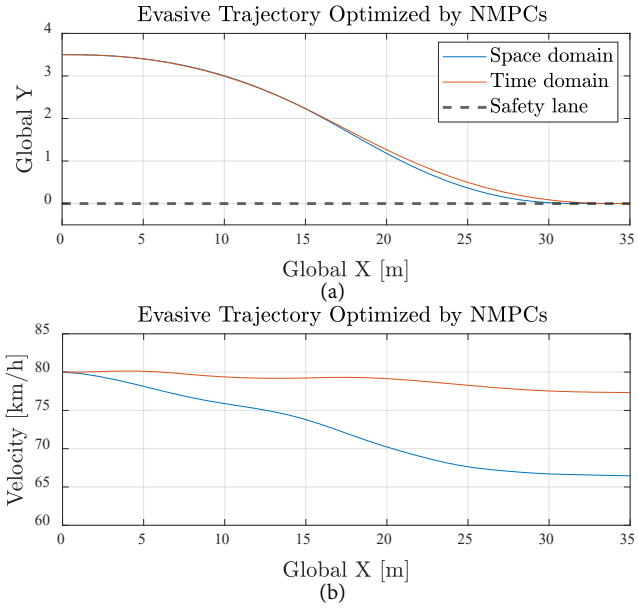

Fig. 4. Evasive vehicle trajectories optimized by the two NMPCs with different stage costs-one with the space domain and the other with the time domain. (a) shows the optimized trajectory, and (b) shows the optimized vehicle velocity.

by the NMPCs, which use the nonlinear model (10) with the prediction horizon set to 50. (a) shows the optimized trajectory, and (b) shows the optimized vehicle velocity. The constraints and the details of the NMPC are not yet introduced, but the difference in the results due to the different stage costs are shown clearly in the figure.

In case of the time domain stage cost, the vehicle moves quickly into the safety lane by maintaining its velocity to achieve a higher convergence rate to the lane. On the other hand, the space domain stage cost reduces the vehicle velocity during the evasive maneuver, as a human driver would, to converge to the lane with a shorter turning radius and thereby resulting in a smaller avoidance area. The proposed stage cost directly penalizes the avoiding area, reducing it by 2.5%. That is, the avoidance distance is reduced by 2.5 m, which is a meaningful improvement that can change the results of collision avoidance.

The remark point of NMPC, compared to other collision avoidance methods, is that NMPC does not require a pre-defined path to avoid collision. The evasive trajectory is also optimized during the control process, while other systems require a pre-defined path, not optimized for the vehicle, to follow. Therefore, generating an evasive path can be omitted for the collision avoidance systems with NMPC, leading to higher evasive performance..

3) Constraints: To secure vehicle stability during the evasive maneuver, safety constraints were applied to the NMPC. These constraints consider the maximum allowable forces of each tire. It is crucial to generate the tire forces that are within the limits of road friction because the control inputs that exceed the friction limit of the road surface will cause the tire to lose grip and cause the vehicle to become unstable [22]. Therefore, constraints are defined to limit the sum of the longitudinal and lateral forces of each wheel during the prediction horizon as follows:

$$\begin{aligned}&\sqrt{\left(F_{x,j}(i|k)\right)^2+\left(F_{y,j}(i|k)\right)^2}\leq\lambda\mu F_{z,j}(i|k)\\&, j=fl,fr,rl,rr, \text{ for } i=0,1,\cdots,N-1\end{aligned}\tag{20}$$

where $F_{x,j}(i|k)$, $F_{y,j}(i|k)$, and $F_{z,j}(i|k)$ are the longitudinal, lateral, and vertical tire forces, respectively, predicted using the nonlinear model (10) within the prediction horizon, and $\lambda \in [0,1]$ is a constraint-tightening parameter to ensure robustness of the NMPC that determines the extent of friction limits applied.

A constraint that prevents the vehicle from crossing the safety lane is also considered. Crossing the safety lane after collision avoidance can lead to secondary accidents with surrounding obstacles. Therefore, constraints that limit the vehicle position are applied as follows:

$$\begin{aligned}&\text{sgn}(y_{\text{pos}}(0|k))y_{\text{pos}}(i|k)\geq 0\\&\text{, for } i=0,1,\cdots,N-1\end{aligned}\tag{21}$$

The constraint maintains the sign of the lateral position of the vehicle, thereby preventing the vehicle from crossing the x-axis within the prediction horizon. Note that the safety lane is the x-axis. In addition, the constraints that only allow braking for the longitudinal tire force inputs are considered as follows:

$$\begin{aligned}&F_{x,j}^{in}(i|k)\leq 0\\&\text{, } j=fl,fr,rl,rr, \text{ for } i=0,1,\cdots,N-1\end{aligned}\tag{22}$$

By combining (20), (21), and (22), constraints are organized as an inequality:

$$\begin{aligned}&g_{\text{ineq}}\left(x(i|k),u(i|k)\right)\leq 0\\&\text{, for } i=0,1,\cdots,N-1\end{aligned}\tag{23}$$

where the constraints can be expressed in terms of states $x(i|k)$ and inputs $u(i|k)$ using equations (1)-(6).

Additionally, a terminal constraint is applied to prevent unexpected results. Because the cost function proposed herein is not a convex function, the optimization problem has various local-minimum solutions, such as the solution making the stage cost (19) converge to 0 by letting $\psi+\beta\rightarrow 90^\circ$ not by regulating $y_{pos}\rightarrow 0$. Therefore, to avoid such results, the terminal constraint is applied to ensure that the lateral position of the vehicle is along the x-axis at the end of the prediction horizon:

$$y_{pos}(N|k)=0\tag{24}$$

The terminal constraint eventually makes the value of the stage cost zero at the end of the prediction horizon; therefore, the terminal cost $P(x(N|k))$ is neglected in (15). (15) represents the sum of the stage costs over the remaining infinite horizon $i=N,\cdots,\infty$; therefore, the proposed terminal constraint also makes the controller more stable [18].

4) Nonlinear optimization: Finally, by applying the nonlinear prediction model (14), cost function (15), and constraints (23), (24), a nonconvex optimization problem for the NMPC can be formulated as follows:

$$\begin{aligned}\min_{U(k)}\quad & J(x(0|k),U(k))\\\text{subject to}\quad & x(i+1|k)=f_d(x(i\mid k),u(i|k))\\& g_{\text{ineq}}(x(i|k),u(i|k))\leq 0\\& y_{pos}(N|k)=0\\& x(0|k)=\bar{x}(k)\\& \text{for } i=0,\cdots N-1\end{aligned}\tag{25}$$

Sequential quadratic programming [40], which is a nonconvex optimization solver, is used to solve the problem, and the first elements of the input sequence are used as control input u_{NMPC} at the nominal vehicle state $\bar{x}(k)$ as follows:

$$u_{\text{NMPC}}(\bar{x}(k))=u(0|k)\tag{26}$$

As mentioned in section I, the NMPC calculates the control inputs to ensure the nominal vehicle model used in the NMPC avoids collision. Therefore, the nominal vehicle model state $\bar{x}(k)$ is used for the initial state of the NMPC, which is obtained by the nonlinear model as follows:

$$\bar{x}(k+1)=f_d\left(\bar{x}(k),u_{\text{NMPC}}(\bar{x}(k))\right)\tag{27}$$

The state of the nominal vehicle model is initialized to the plant vehicle state at the initiation of the collision avoidance system; the nonlinear model then calculates it during the control process.

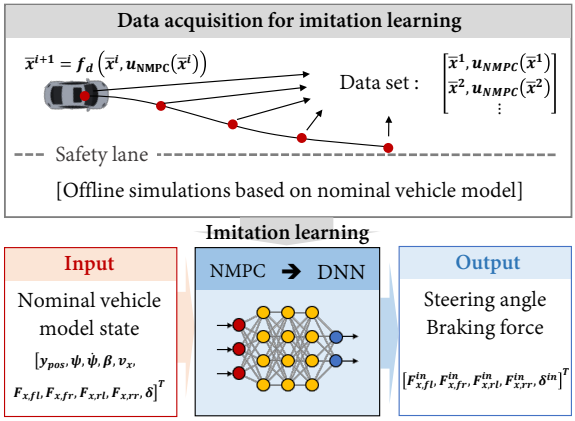

Fig. 5. Imitation learning architecture replacing the NMPC.

TABLE I
INITIAL CONDITIONS FOR THE OFFLINE NOMINAL VEHICLE MODEL-BASED SIMULATION.

State	Range	State	Range
y_{pos} [m]	2, 3, 4	ψ [deg]	-3, 0, 3
$\dot{\psi}$ [deg/s]	-2, 0, 2	β [deg]	-0.5, 0, 0.5
v_x [km/h]	70, 80, 90	F_x [N]	-1000, 0
δ [deg]	-1, 0, 1	-	-

C. Behavioral cloning

Behavioral cloning was adopted to enable the NMPC to be imitated by a DNN via supervised learning, mitigating the computation load of the controller, as shown in Fig. 5. Although advanced IL methods such as DAgger and inverse reinforcement learning can be used, this study applied behavioral cloning due to its simple structure and the verified imitation performance of the NMPC by previous studies. In case of other methods are used instead of behavioral cloning, the structure proposed in this study can be applied the same.

1) Data acquisition: Because the proposed NMPC controlled the nominal vehicle model, offline simulations were generated based on the nominal vehicle model, and the training data set was obtained. The inputs X_{DNN} and outputs Y_{DNN} of the data set are formulated as follows:

$$\text{Data set} : [X_{\text{DNN}}, Y_{\text{DNN}}] = \begin{bmatrix} \bar{x}^1 & u_{\text{NMPC}}(\bar{x}^1) \\ \bar{x}^2 & u_{\text{NMPC}}(\bar{x}^2) \\ \vdots & \vdots \end{bmatrix} \tag{28}$$

where $\bar{x}^i$ for $i = 1, 2, \cdots$ are the sample nominal vehicle states, and $u_{\text{NMPC}}(\bar{x}^i)$ is the NMPC control input obtained by (25). As mentioned earlier, no experiments involving the plant vehicle are needed; instead, data are generated offline through the nominal vehicle model-based simulation as follows:

$$\bar{x}^{i+1} = f_d(\bar{x}^i, u_{\text{NMPC}}(\bar{x}^i)) \text{ for } i = 1, \cdots \tag{29}$$

Offline simulations were performed with various initial conditions, as summarized in Table I, until the nominal vehicle model converged sufficiently to the safety lane. A total of 72,900 data were used for training. The initial conditions represent the vehicle states and driver's inputs before initiating the collision avoidance system. For the braking forces made by the driver's input, the ratio of the force of each wheel is set constant considering the braking ratio $\eta = 0.4$ between the front and rear axles as follows:

$$F_{x,fl} = F_{x,fr} = F_x \tag{30a}$$
$$F_{x,rl} = F_{x,rr} = \eta F_x \tag{30b}$$

TABLE II
RESULTS OF BAYESIAN OPTIMIZATION FOR SELECTING HYPERPARAMETERS OF THE DNN

Rank	Loss ($\times 10^4$)	Hidden layers	Nodes	Learning rate
1	29.9	3	43	$10^{-3.00}$
2	31.0	3	46	$10^{-3.12}$
3	32.0	9	42	$10^{-2.68}$
⋮	⋮	⋮	⋮	⋮

The inputs and outputs of the data sets were standardized for better training, and they were split into training and validation data sets in the ratio of 8:2, used for training the DNN and optimizing the hyperparameters, respectively. The trained DNN was later applied in the CarSim-based human-vehicle interactive simulation. Note that the DNN was pre-trained only using the data set obtained offline and applied to the plant vehicle.

2) Supervised learning: A fully connected DNN, with 10 inputs and 5 outputs as shown in Fig. 5, was used as previous studies [33]–[35]. Adaptive moment estimation (Adam) [41], with gains as [42], was used to optimize the DNN weights. The weights were optimized, thereby minimizing the loss function, which was set as the mean squared error (MSE) between the actual $u_{\text{NMPC}}(\bar{x}^i)$ and imitated control input $u_{\text{DNN}}(\bar{x}^i)$ as follows:

$$\text{MSE} = \frac{1}{N_B} \sum_{i=1}^{N_B} \left(u_{\text{NMPC}}(\bar{x}^i) - u_{\text{DNN}}(\bar{x}^i) \right)^2 \tag{31}$$

where N_B is the batch size for the training process set as 256. The hyperparameters of the DNN learning process, such as the number of hidden layers, nodes, and learning rate, were optimized by the Bayesian optimization (BO) [43] with the expected improvement as the acquisition function. The results are listed in Table II, and the DNN structure with the greatest performance was used for IL. To prevent overfitting, the training was terminated using early stopping, which stops the learning if the loss function does not improve for a certain number of epochs.

Further verification of the reliability of the DNN is needed to guarantee the safety of the proposed system. Such strict verifications are major challenges in learning control fields [44], [45], including not only imitation learning but also reinforcement learning and data-driven controls. In this study, it is assumed that the data set can cover the state space fully; therefore, the trained DNN's reliability is considered sufficient to be applied in the system. This is because the limits on access to training data are removed as the data set is based on the offline simulation. The data was sufficiently collected, as

shown in Table I. However, rigorous verification for reliability is still needed and therefore is left for future work of this study.

III. Input Dimensionalization

This section explains the input dimensionalization process, which makes the proposed IL structure robust to parameter variations.

A. Objective

After the NMPC is imitated by a DNN,

$$u_{\text{NMPC}}(\bar{x}(k)) \rightarrow u_{\text{DNN}}(\bar{x}(k)) \tag{32}$$

an input dimensionalization (ID) process is performed to overcome the weakness of IL that cannot handle changes in model parameters. If the plant vehicle parameters change, safety constraint satisfaction may not be guaranteed when the DNN is directly applied to the controller. This can lead to dangerous situations caused by the unstable behavior of the vehicle.

Therefore, the ID modifies the control input $u_{\text{DNN}}(\bar{x}(k))$, to make the plant vehicle safer under such parameter variations by considering the changed parameters. The targets of parameter variations are m, I_z, l_f, h, and C_0, which are used in the NMPC. For variations in these parameters, the control input is modified to satisfy the constraint (20) because satisfying the friction limit constraint during evasive maneuvers is crucial to vehicle stability. To do so, the aim of the ID is to keep the grip ratio of the friction limits utilized for each tire of the plant vehicle identical to that of the nominal vehicle model. The grip ratio can be expressed as follows:

$$\frac{\sqrt{\left(F_{x,j}\right)^2+\left(F_{y,j}\right)^2}}{\mu F_{z,j}}, \text{ for } j = fl, fr, rl, rr \tag{33}$$

When the DNN is directly applied to the controller, the grip ratio may surpass the friction limit, for example, because of the reduction in the vertical force $F_{z,j}$ due to the decreased mass of the plant vehicle. On the other hand, when the DNN employs ID, the control input is modified, for example, reducing the braking force $F_{x,j}$ to match the grip ratio of the plant vehicle with that of the nominal model.

B. Methodology

Suitable results can be achieved by ensuring that the nominal model and plant vehicle have identical longitudinal and lateral force ratios for the maximum allowable force of each tire. For the nominal model, the ratio can be calculated considering the nominal vehicle state $\bar{x}(k) = [\bar{x}_v(k), \bar{u}_v(k)]^T$ using the equations (1)-(6) as follows:

$$\begin{aligned} h_{\text{Nom}}(\bar{x}_v(k), \bar{u}_v(k)) = \Bigg[&\frac{\bar{F}_{x,fl}(k)}{\mu \bar{F}_{z,fl}(k)}, \frac{\bar{F}_{x,fr}(k)}{\mu \bar{F}_{z,fr}(k)}, \\ &\frac{\bar{F}_{x,rl}(k)}{\mu \bar{F}_{z,rl}(k)}, \frac{\bar{F}_{x,rr}(k)}{\mu \bar{F}_{z,rr}(k)}, \frac{\bar{F}_{y,fl}(k)}{\mu \bar{F}_{z,fl}(k)} \Bigg]^T \end{aligned} \tag{34}$$

where $\bar{F}_{x,j}(k)$, $\bar{F}_{y,j}(k)$, and $\bar{F}_{z,j}(k)$ for $j = fl, fr, rl, rr$ are the longitudinal, lateral, and vertical forces acting on each tire of the nominal vehicle model. Only the front left tire is considered for the lateral force because modifying the steering angle input can only change the ratio of the front tires, and the ratios for the left and right tires are identical as the slip angles are identical (5a). The remaining lateral force ratio of the rear tires is supplemented by the feedback controller, which is introduced in section IV. Here, $h_{\text{Nom}}(x_v, u_v)$ is obtained using the nominal parameters m, I_z, l_f, h, and C_0.

Then, $\tilde{u}_v(k)$ can be obtained solving the following equation:

$$h_{\text{True}}\left(\hat{x}_v(k), \tilde{u}_v(k)\right)) = h_{\text{Nom}}\left(\bar{x}_v(k), \bar{u}_v(k)\right) \tag{35}$$

where $\hat{x}_v$ is a portion of the state of the plant vehicle, and $h_{\text{True}}(x_v, u_v)$ considers the true model parameters, namely, $\hat{m}$, $\hat{I_z}$, $\hat{l_f}$, $\hat{h}$, and $\hat{C_0}$. The above equation implies that if the state of the plant vehicle is controlled as follows:

$$\hat{x}(k) = [\hat{x}_v(k), \hat{u}_v(k)]^T \rightarrow [\hat{x}_v(k), \tilde{u}_v(k)]^T \tag{36}$$

The grip ratio utilized during the evasive maneuver is kept the same as the ratio obtained from the NMPC, even under parameter variations.

Therefore, the modified input $u_{\text{FF}}(k)$, which is obtained by ID, is calculated to ensure that the vehicle state satisfies the above equation. However, because the input is delayed by the dynamics of the lower controller (8), these conditions cannot be satisfied at the current step k. Alternatively, input $u_{\text{FF}}(k)$ ensures that the predicted state of the plant vehicle at step $k+1$ based on step k satisfies these conditions. This input is given as follows:

$$\begin{aligned} \hat{x}(1|k) &= [\hat{x}_v(1|k), \hat{u}_v(1|k)]^T \\ &\rightarrow [\hat{x}_v(1|k), \tilde{u}_v(1|k)]^T \end{aligned} \tag{37}$$

where $\tilde{u}_v(1|k)$ can be obtained by solving the following equation, which is composed of the predicted states of the plant vehicle and the nominal vehicle model:

$$\begin{aligned} h_{\text{True}}(\hat{x}_v(1|k), &\tilde{u}_v(1|k)) \\ &= h_{\text{Nom}}(\bar{x}_v(1|k), \bar{u}_v(1|k)) \end{aligned} \tag{38}$$

Therefore, by calculating the predicted states using (14):

$$\begin{aligned} \hat{x}(1|k) &= [\hat{x}_v(1|k), \tilde{u}_v(1|k)]^T \\ &= \hat{f}_d\left(\hat{x}(k), u_{\text{FF}}(k)\right) \end{aligned} \tag{39a}$$

$$\begin{aligned} \bar{x}(1|k) &= [\bar{x}_v(1|k), \bar{u}_v(1|k)]^T \\ &= f_d\left(\bar{x}(k), u_{\text{DNN}}(\bar{x}(k))\right) \end{aligned} \tag{39b}$$

where $\hat{f}_{d,x}(x, u)$ is the discretized nonlinear model (10) applied with the true model parameters, $u_{\text{FF}}(k)$ satisfy the following equation:

$$\tilde{u}_v(1|k) = e^{-\frac{T}{\tau}} \hat{u}_v(k) + \left(I - e^{-\frac{T}{\tau}}\right) u_{\text{FF}}(k) \tag{40}$$

and can be obtained as follows:

$$u_{\text{FF}}(k) = \frac{\tilde{u}_v(1|k) - e^{-\frac{T}{\tau}} \hat{u}_v(k)}{I - e^{-\frac{T}{\tau}}} \tag{41}$$

By the aforementioned ID process, the control input obtained from the DNN is modified to satisfy the friction limit constraints even under parameter variations, thereby ensuring robustness of the IL algorithm to parameter changes.

Using the same method, the future feedforward input sequence $U_{\text{FF}}(k)$ can also be predicted as follows:

$$U_{\text{FF}}(k) = [u_{\text{FF}}(0|k), u_{\text{FF}}(1|k), \cdots]^T \tag{42}$$

with $u_{\text{FF}}(0|k) = u_{\text{FF}}(k)$. The following equations hold:

$$u_{\text{FF}}(i|k) = \frac{\tilde{u}_v(i+1|k) - e^{-\frac{T}{\tau}}\hat{u}_v(i|k)}{I - e^{-\frac{T}{\tau}}} \tag{43}$$

where $\tilde{u}_v(i+1|k)$ can be obtained by solving the following equation:

$$\begin{aligned} &h_{\text{True}}(\hat{x}_v(i+1|k), \tilde{u}_v(i+1|k)) \\ &\qquad = h_{\text{Nom}}(\bar{x}_v(i+1|k), \bar{u}_v(i+1|k)) \end{aligned} \tag{44}$$

The predicted states are calculated as follows:

$$\begin{aligned} \hat{x}(i+1|k) &= [\hat{x}_v(i+1|k), \tilde{u}_v(i+1|k)]^T \\ &= \hat{f}_d\left(\hat{x}(i|k), u_{\text{FF}}(i|k)\right) \end{aligned} \tag{45a}$$

$$\begin{aligned} \bar{x}(i+1|k) &= [\bar{x}_v(i+1|k), \bar{u}_v(i+1|k)]^T \\ &= f_d\left(\bar{x}(i|k), u_{\text{DNN}}(\bar{x}(i|k))\right) \end{aligned} \tag{45b}$$

Such a future feedforward input sequence is used in the feedback controller for linearizing the nonlinear model; this step is introduced in the next section.

IV. Feedback Controller

This section introduces the feedback controller in the control structure as shown in Fig. 1. This controller regulates the error between the plant vehicle and nominal vehicle model.

A. Objective

As the NMPC, imitated by the DNN, controls the nominal vehicle model during evasive maneuver, an additional feedback controller is needed to regulate the error between the plant vehicle and the nominal vehicle model. Without such a controller, the plant vehicle will deviate from the expected evasion maneuver, and the error between them will accumulate during the control process.

To match the lateral and longitudinal evasive maneuvers, the y_{pos}, and v_x errors are regulated between the plant vehicle and nominal model. Further, $F_{y,rl}/F_{z,rl}$ error is regulated to match the lateral grip ratio of the plant vehicle and the nominal model-this regulation is not possible by the ID process. Since the lateral grip ratio are identical for the left and right tires, only the rear left tire is considered (5b). Therefore, y_{pos}, v_x, and $F_{y,rl}/F_{z,rl}$ of the plant vehicle are controlled by the feedback controller $u_{\text{FB}}(k)$ to track the values of the nominal vehicle model.

The feedback controller should calculate the control input of the multi-input-multi-output system with a low computation load and should be able to handle nonlinearities in the vehicle dynamics. Therefore, this study applied a finite-horizon linear quadratic (LQ) controller [18] for the feedback controller. It can handle nonlinearities by applying a linearized time-varying (LTV) model and can calculate the optimal control input obtained by solving an unconstrained convex problem with a low computation load.

B. Finite-horizon LQ controller

The finite-horizon LQ controller is similar to the NMPC in that it optimizes the control input by minimizing the cost function considering the prediction of the future state of the vehicle along the finite-horizon. Therefore, an LTV is derived from the nonlinear model for use as the prediction model along the prediction horizon N_{LQ}.

1) LTV prediction model: The LTV prediction model is obtained by linearizing the nonlinear model (10), which is expressed as follows:

$$x(k+1) = \hat{f}_d(x(k), u_{\text{FF}}(k) + u_{\text{FB}}(k)) \tag{46a}$$

$$y(k) = \hat{g}(x(k)) \tag{46b}$$

where the output function $\hat{g}(x(k))$ is obtained by considering equations (1)-(6) with the true plant vehicle parameters, and the state, feedback control input, output vectors are as follows:

$$x = [x_v, u_v]^T \tag{47a}$$

$$y = \left[y_{\text{pos}}, v_x, \frac{F_{y,rl}}{F_{z,rl}}\right]^T \tag{47b}$$

$$u_{\text{FB}} = \left[F^{\text{FB}}_{x,fl}, F^{\text{FB}}_{x,fr}, F^{\text{FB}}_{x,rl}, F^{\text{FB}}_{x,rr}, \delta^{\text{FB}}\right]^T \tag{47c}$$

By linearizing the nonlinear model, an LTV prediction model can be obtained as follows:

$$x(i+1|k) = A_{i|k}x(i|k) + B_{i|k}u_{\text{FB}}(i|k) + E_{i|k} \tag{48a}$$

$$y(i|k) = C_{i|k}x(i|k) \tag{48b}$$

$$\text{, for } i = 0, 1, \cdots, N_{LQ} - 1$$

The linearized model matrices are obtained by linearizing the nonlinear model around the predicted future state along the finite-horizon to reduce the linearization error [22] because the future vehicle state can be predicted by the future feedforward input sequence $U_{\text{FF}}(k)$. Thus, the model matrices are calculated as follows:

$$A_{i|k} = \nabla_x \hat{f}_{d,x}(x)|_{\hat{x}(i|k)},\ B_{i|k} = B \tag{49a}$$

$$C_{i|k} = \nabla_x \hat{g}_x(x)|_{\hat{x}(i|k)} \tag{49b}$$

$$E_{i|k} = \hat{f}_{d,x}(\hat{x}(i|k)) + Bu_{\text{FF}}(i|k) \tag{49c}$$

The predicted future states are obtained using the future feedforward control inputs as follows:

$$\hat{x}(i+1|k) = \hat{f}_d\left(\hat{x}(i|k), u_{\text{FF}}(i|k)\right) \tag{50a}$$

$$\hat{x}(0|k) = \hat{x}(k) \tag{50b}$$

$$\text{, for } i = 0, 1, \cdots, N_{LQ} - 1$$

2) Cost function: A cost function $J(\hat{x}(k), U_{\text{FB}}(k))$ for regulating the output error between the plant vehicle and the nominal vehicle model is designed as follows:

$$\begin{aligned} &J(x(0|k)(k), U_{\text{FB}}(k)) \\ &= \sum_{i=0}^{N_{LQ}-1} \Big(\left(\bar{y}(i|k) - y(i|k)\right)^T Q_y \left(\bar{y}(i|k) - y(i|k)\right) \\ &+ u_{\text{FB}}(i|k)^T R_{u_{\text{FB}}} u_{\text{FB}}(i|k)^T \\ &+ \Delta u_{\text{FB}}(i|k)^T R_{\Delta u_{\text{FB}}} \Delta u_{\text{FB}}(i|k)^T \Big) \end{aligned} \tag{48}$$

where Q_y, $R_{u_{\text{FB}}}$, and $R_{\Delta u_{\text{FB}}}$ are positive definite matrices that penalize the output difference, feedback input, and feedback input change, respectively. $U_{\text{FB}}(k)$ is the future feedback input sequence that will be optimized by the LQ controller as follows:

$$U_{\text{FB}}(k) = \left[u_{\text{FB}}(0|k), \cdots, u_{\text{FB}}\left(N_{LQ}-1|k\right)\right]^T \tag{49}$$

$\Delta u_{\text{FB}}(i|k)$ is calculated in the same manner as shown in (17), and $\bar{y}(i|k)$ is the reference output value from the nominal vehicle model:

$$\bar{x}(i+1|k) = f_d\left(\bar{x}(i|k), u_{\text{DNN}}(\bar{x}(i|k))\right) \tag{50a}$$

$$\bar{y}(i|k) = g(\bar{x}(i|k)) \tag{50b}$$

$$\bar{x}(0|k) = \bar{x}(k) \tag{50c}$$

$$\text{, for } i = 0, 1, \cdots, N_{LQ}-1$$

Here, the output function $g(x(i|k))$ considers the nominal model parameters.

Therefore, by combining the LTV prediction model (46) and cost function (51), an unconstrained convex optimization problem for the finite-horizon LQ controller can be formulated as follows:

$$\begin{aligned} \min_{U_{\text{FB}}(k)} \quad & J(x(0|k), U_{\text{FB}}(k)) \\ \text{subject to} \quad & x(i+1|k) = A_{i|k}x(i|k) + B_{i|k}u_{\text{FB}}(i|k) + E_{i|k} \\ & y(i|k) = C_{i|k}x(i|k) \\ & \text{for } i = 0, \cdots N_{LQ}-1 \\ & x(0|k) = \hat{x}(k) \end{aligned} \tag{51}$$

The above convex problem can be solved using the batch approach. The detailed procedure is skipped for brevity; for details, see [18]. Finally, the first elements of the optimized input sequence are used for the feedback input as follows:

$$u_{\text{FB}}(k) = u_{\text{FB}}(0|k) \tag{52}$$

Note that the purpose of the feedback controller is to regulate the difference between the nominal vehicle model and plant vehicle. Other types of controllers that can perform the same task can be applied instead of the proposed finite-horizon LQ controller.

V. Simulation Verification

CarSim-based human-vehicle interactive simulation experiments were performed to verify the performance of the proposed algorithm.

A. Configuration

The proposed collision avoidance system aims to assist the driver by taking over the control inputs of the vehicle in a collision risk situation. Therefore, a CarSim-based human-vehicle interactive simulation was performed to verify the performance of the proposed algorithm in such situations. CarSim, a high-fidelity vehicle simulator, was connected to Thrustmaster T150 pro, which allowed a driver to control the plant vehicle directly using the steering wheel and pedals. The algorithm was run in MATLAB on a personal computer equipped with AMD Ryzen 9 3900X and 64 GB RAM. The simulation was performed in real-time using the Simulink desktop real-time toolbox [46] provided by MATLAB, which reports errors if the algorithm cannot run in real-time.

TABLE III
Control parameters of the proposed algorithm.

Parameter	Value
$T\,[sec]$	0.05
λ	0.7
N	50
Q_{area}	10
R_u	diag(5e-9, 5e-9, 5e-9, 5e-9, 0)
$R_{\Delta u}$	diag(1e-7, 1e-7, 1e-7, 1e-7, 10)
N_{LQ}	10
Q_y	diag(10, 500, 10)
$R_{u_{\text{FB}}}$	diag(1e-6, 1e-6, 1e-4, 1e-4, 20)
$R_{\Delta u_{\text{FB}}}$	diag(1e-5, 1e-5, 1e-5, 1e-5, 10)

TABLE IV
Three control structures in the experiment.

Type	Components of the control structure
Proposed	DNN + Feedback + ID
Case 1	DNN (plant vehicle's state)
Case 2	DNN + Feedback
Case 3	LMPC

A front-wheel-driven E-class sedan in CarSim software was used as the vehicle. True parameters were assumed to be known in ID, and the feedback controller with an error of 5% referring to existing parameter estimation methods [47], [48]. Also, time constants for dynamics of the lower controller in (8) were set as $\tau_{F_x} = 0.06$ and $\tau_\delta = 0.1$. During the experiment, a human driver drives the vehicle with a velocity of 80 km/h representing normal driving; subsequently, the proposed system intervenes and takes over the control inputs to avoid a collision. After the vehicle reaches the safety lane, the collision avoidance system is terminated, and the driver resumes driving. The overall scenario of the experiment is shown in Fig 6. The safety lane was set to be 3.5 m apart from the lane where the vehicle traveled, representing an emergency single-lane change. Note that 3.5 m is not included in the conditions for training the DNN shown in Table I.

A precise decision algorithm would be necessary for initiating the avoidance system. Future trajectories of the obstacles can be predicted [49] and used to decide whether or not the ego vehicle is in danger of colliding with them. If the decision algorithm concludes that the obstacle will collide with the ego vehicle, a safety lane [50] is provided to the proposed collision avoidance algorithm to evade the vehicle from collisions safely. However, this is beyond the scope of this work, and to simplify the scenario, the avoidance system is initiated and terminated when the vehicle reaches a specific position; global x 100 m and 150 m. The control parameters used in the proposed algorithm are listed in Table III.

As shown in Table IV, three collision avoidance systems were compared with the proposed algorithm. In Case 1, the DNN was applied directly to the plant vehicle without ID and feedback control. This case is included in the comparison to

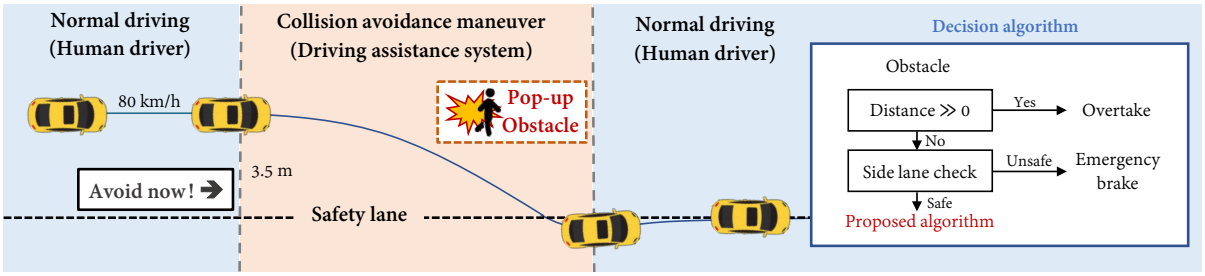

Fig. 6. Overall experimental scenario. The human driver drives the vehicle first, and the collision avoidance system is initiated as the vehicle is being driven. After the vehicle reaches the safety lane, the operation of the system is terminated, and the driver resumes driving.

TABLE V
NOMINAL AND TRUE VEHICLE MODEL PARAMETERS.

Parameter	Value	
	Nominal	True
m [kg]	1830	1630
I_z [kg · m^2]	3770	3389
l_f [m]	1.41	1.28
h [m]	0.51	0.46
C_0 [−]	20.9	14.3

show that it requires experiments with plant vehicles to obtain the training data for the DNN. In Case 2, DNN is used with a feedforward feedback structure without ID to show that such a structure can allow the DNN to be trained by simulation results based on an offline nominal vehicle model; however, it is still vulnerable to parameter changes. Finally, Case 3 is the conventional collision avoidance system with LMPC that controls steering only with a predefined collision-free path. It is compared to show the effectiveness of applying NMPC to collision avoidance rather than LMPC. This study referred to [4] for path generation and [5] for the controller. Unlike the DNN, estimated true model parameters were directly applied to the controller. Details can be referred to in each citation.

B. Comparisons

Comparison experiments on collision avoidance for a vehicle were performed. The true parameters of the vehicle plant were set differently from the nominal vehicle model as indicated in Table V to verify robustness against model parameter changes. Four collision avoidance systems as Table IV were applied, and their performances were compared. In addition, evasive maneuvers by only human drivers without any intervention from the avoidance system were examined. In this examination, the human drivers tried their best to move the vehicle to the safety lane by steering and braking. Fig. 7 shows the result of the comparison experiment. (a) shows the vehicle's evasive trajectory, and (b)-(e) show the grip ratio of each tire during the evasion maneuver. Here the grip ratio was calculated using (33) with (1)-(6). As the grip ratio of each tire reached nearly to 1 during the evasion, it can be seen that four controllers evaded the car urgently using the tire up to the nonlinear region [37].

In Case 3, the vehicle followed the pre-defined collision-free path and successfully converged to the safety lane. LMPC

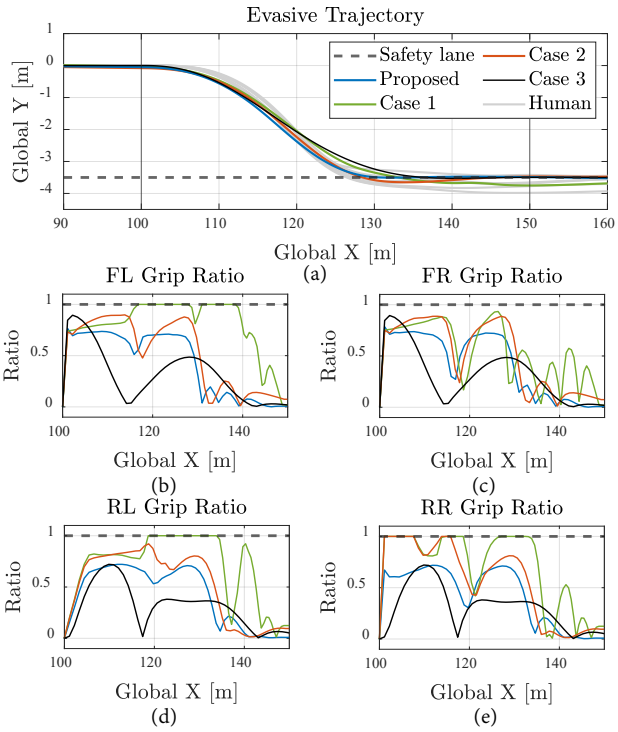

Fig. 7. Experimental results of comparison with the existing imitation learning methods. (a) The vehicle trajectory, (b)-(e) grip ratios of each tire (front left, front right, rear left, and rear right, respectively.

showed great tracking results, which many previous studies have also verified; however, the evasive trajectory showed the largest avoidance area compared to the other methods. The performance difference was clearly shown in the global x 115-130 m, where the proposed system increased the curvature of the evasive trajectory to decrease the avoidance area, while Case 3 did not. It controlled only the steering to restrict the vehicle behavior in a linear region, where dominant lateral forces were accompanied during the evasion. Since the slip angles of the left and right tires were the same and lateral forces were proportional to vertical forces, the grip ratio of the left and right tires came out the same. Uneven usage of grip ratio was shown with low usage of grip ratio at the exit of the evasion, which means the controller did not utilize the avoidance performance of the vehicle entirely. Because the nonlinear dynamics of the vehicle were not considered in the pre-defined path or the controller, the evasive maneuver was

TABLE VI
AVOIDANCE AREA AND MAXIMUM GRIP RATIO OF FIG. 7.

Method	Performance		Method	Performance	
	Area	Ratio		Area	Ratio
Proposed	92.5	0.78	Case 2	94.9	1.00
Case 1	101.0	1.00	Case 3	101.8	0.89

degraded compared to the proposed method.

On the other hand, IL-based controllers (Case 1, Case 2, and Proposed) evaded the vehicle to the safety lane with a smaller avoidance area than Case 3. The potential of applying IL to the emergency collision avoidance system was verified. However, the drawbacks of cases 1 and 2 were shown. Case 1 showed severe violations in the safety constraints as shown in Fig. 7(b)-(e). The controlled vehicle became unstable in the global x coordinates range of 120-140 m as more than two wheels were saturated, resulting in a greater overshoot in the tracking results. Because the DNN was trained to control the nominal vehicle model, not the plant vehicle, the vehicle was not controlled properly to be maneuvered to the safety lane. This means that experiments involving real vehicle plants are necessary if the DNN is to be directly applied to the vehicle.

On the contrary, Case 2 and the proposed algorithm controlled the vehicle to the safety lane as intended by the DNN. DNN controlled the nominal vehicle model, and the feedback controller regulated the difference between the nominal vehicle model and the plant vehicle. Hence, the vehicle maneuvered to the safety lane precisely, with much smaller trajectory deviations from the safety lane than in Case 1. However, the vehicle parameter variations were not considered in Case 2, and therefore, the safety constraints were shown to be more vulnerable compared to the proposed algorithm.

As shown in Fig. 7(e), the grip ratio of Case 2 reached the boundary, although the safety constraint was set conservatively by selecting $\lambda = 0.7$. The reason is that the feedforward inputs were made only considering the nominal parameters. Because the plant vehicle mass was smaller and the CG point was closer to the front axle than the nominal vehicle model, the vertical forces of the tires had lower values than the ones expected by the nominal vehicle model, especially for the rear tires. It resulted in the deviation of the rear grip ratios during the evasion, showing unintentionally high values. Because the number of tires that violated the constraint was only one, the vehicle could be avoided to the safety lane. However, such moments may violate the vehicle stability, leading to unstable vehicle behavior, as in Case 1. Therefore, more conservative control strategies are demanded to apply collision avoidance systems with Case 2 under such parameter changes, which results in collision avoidance ability degradation.

On the contrary, parameter changes were considered in the proposed algorithm by modifying DNN control inputs suitable to the plant vehicle through ID. ID modified the control inputs considering the changed model parameters to match the grip ratio of the plant vehicle with that of the nominal model. As a result, grip ratio of each tire were close to 0.7 as intended by the NMPC, showing greater margin to vehicle stability compared to other methods. Table VI is the avoidance

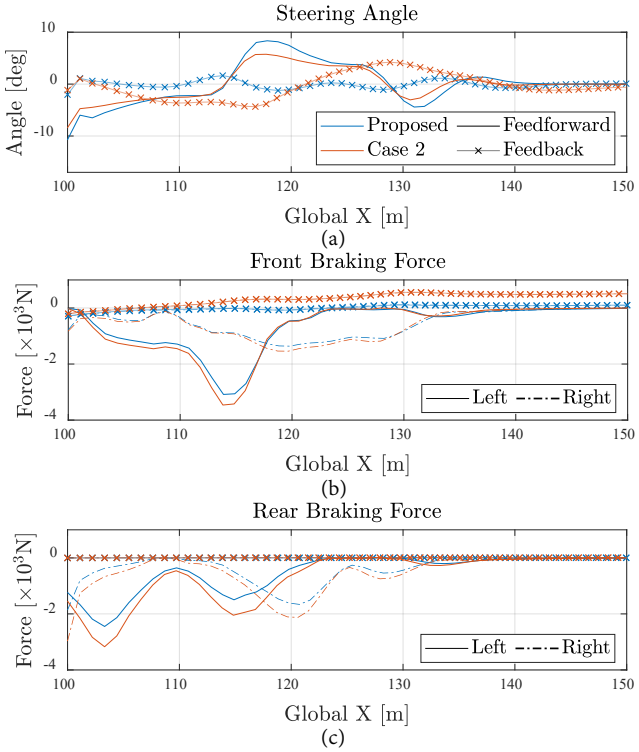

Fig. 8. Control inputs modified by ID considering the plant vehicle parameters. (a) The steering angle, and (b), (c) front/rear braking force inputs, respectively.

area and the maximum tire grip ratio used by each method during the maneuver. Here, the area was re-scaled by setting the human driver's average avoidance area to 100 for better comparison. The table shows that the proposed system showed the smallest avoidance area with the lowest tire grip ratio used. It showed greater avoidance performance while guaranteeing more margin in the tire's maximum grip ratio compared to other methods.

C. Robustness to parameter variations

The results of ID in Fig. 7 and its role in obtaining robustness to parameter variations are further analyzed. Fig. 8 shows the proposed algorithm's feedforward and feedback control inputs compared with Case 2, where the ID is not applied. (a) shows the steering angle input, (b) and (c) show the front/rear braking force, respectively.

As shown in Fig. 8(b) and (c), ID reduced the tires' braking forces to match the trip ratio of the tires to the nominal vehicle model considering the reduced plant vehicle's mass. If ID did not reduce the braking forces, tires could have been saturated with excessive tire forces as in Case 2 in Fig. 7(e). The steering angle was also increased, considering the decreased cornering stiffness. ID considered the changed model parameters to equalize the grip ratio to the nominal vehicle model; therefore, the proposed algorithm could be able to handle model parameter changes and gain robustness compared to Case 2. Furthermore, due to such input modifications by ID, the plant vehicle followed the intent of the DNN better under

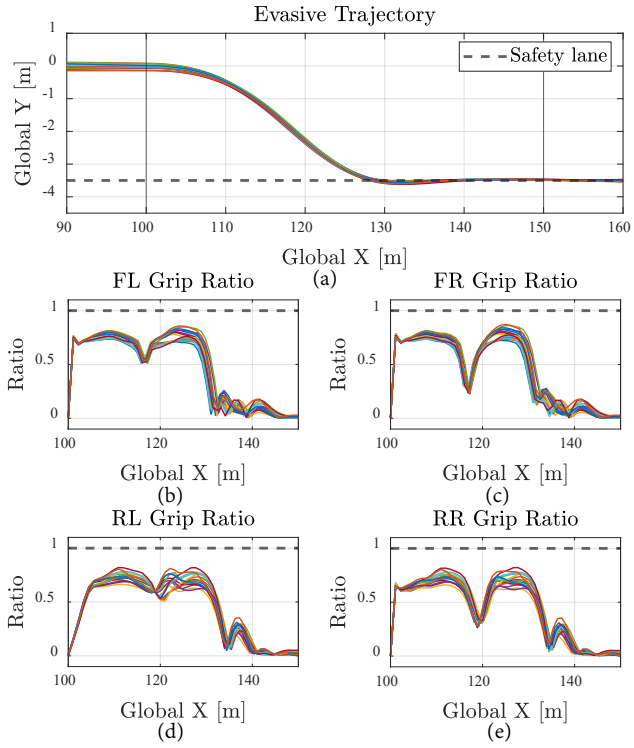

Fig. 9. Experimental results under various parameter changes (a) is the vehicle trajectory, (b)-(e) are the grip ratio of each tire, front left, front right, rear left, rear right, respectively.

TABLE VII
NOMINAL VEHICLE MODEL PARAMETERS AND VARIATIONS.

Parameter	Value	
	Nominal	True
m [kg]	1830	1630, 2030
I_z [kg · m^2]	3770	3389, 4160
l_f [m]	1.41	1.28, 1.55
h [m]	0.51	0.46, 0.56
C_0 [−]	20.9	14.3, 20.9

parameter changes. This can be analyzed by the magnitude of the feedback control inputs, which tried to regulate the error between the nominal vehicle model and the plant vehicle. As shown in Fig. 8, feedback control inputs were shown smaller in the proposed algorithm compared to Case 2, meaning that ID reduced the gap between the plant vehicle and the nominal vehicle model due to model parameter changes.

To further verify the robustness of parameter changes of the proposed structure, experiments under every parameter combination in the value mentioned in Table VII were held. Fig. 9 shows the results, and sub-figures are the same as Fig 7. As mentioned in the previous subsection, ID modified the control inputs to match the grip ratio between the plant vehicle and the nominal vehicle model. Therefore, satisfaction with the safety constraints was shown in (b)-(e), even under parameter changes. Unlike baselines shown in Fig. 7, the maximum values of the grip ratios of each wheel were shown close to 0.7, which is intended by the DNN showing robustness to parameter variations. Without ID, the feedforward controller would

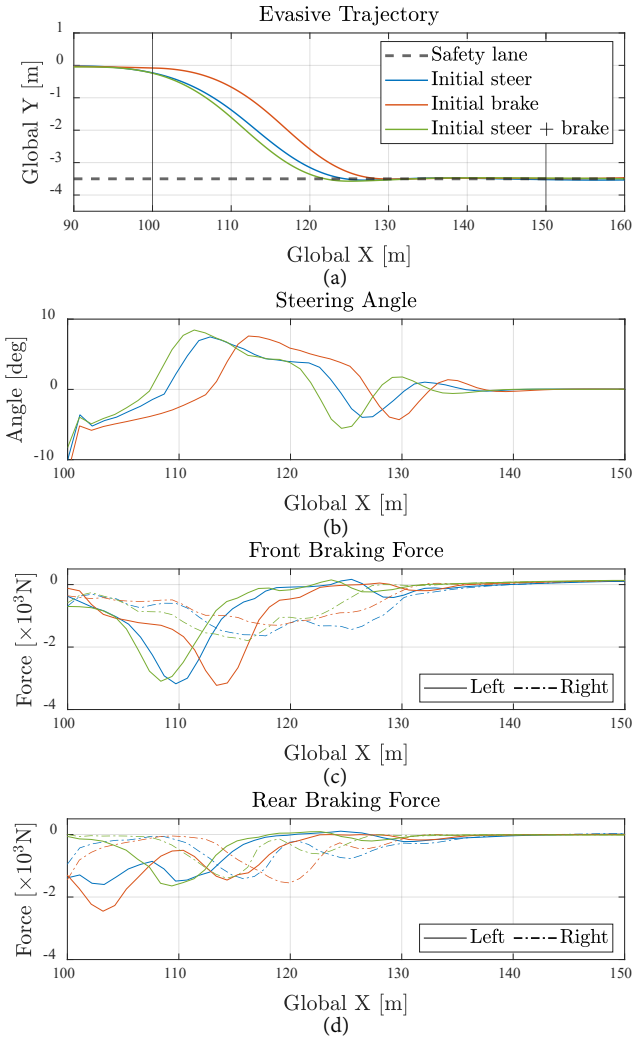

Fig. 10. Control input for collision avoidance under human driver's initial input.

calculate the same control inputs for all parameter variations, resulting in unstable vehicle behavior due to discrepancies between the nominal model and the plant, as in Cases 1 and 2.

D. Collision avoidance under human driver's initial input

Sensitivity analysis for the initiation point of the proposed algorithm was verified by initiating the collision avoidance system under the human driver's initial input. Because the DNN was trained for various nominal states starting from different initial conditions, as Table I, the controller successfully controlled the vehicle regardless of the different initiation states. Fig. 10 shows the collision avoidance system results with various initial human driver inputs; initial steer, initial brake, and initial steer & brake. (a) shows the evasive trajectory, and (b)-(d) show the control inputs made by the system.

As shown in the figure, a smaller evasive area was shown under initial steering than initial braking intuitively. Moreover, initial steering with braking showed the least evasive area because of the reduced speed during the evasive maneuver.

The braking forces were distributed to each tire, considering the friction limits. Because the vertical forces of the left tires were bigger than the right tires during the evasion at global x position 105-115 m, larger braking forces for the left tires were made. Furthermore, the braking force of the front tire was set small at the beginning of avoidance because the steering maneuver of the front tire demanded lateral force. On the contrary, large braking forces were initially applied in the rear tires because no initial lateral forces were acting on the tire. When the sign of the steering angle changed, the controller increased the front wheel braking force using the remained grip ratio to decrease the vehicle velocity.

The control algorithm evaded the vehicle to the safety lane by steering and distributing braking forces of each tire which would have been difficult or even impossible for a human driver only using a single brake pedal. Overall, the simulation was held in real-time due to the low computational load of the DNN, replacing the NMPC. The overall maximum computation time of the proposed control structure, including the ID and feedback controller, was 8 ms, below the sampling time interval of 50 ms. No real-time error was reported in the experiment, verifying the proposed algorithm's real-time capability.

VI. Conclusion & Future work

This paper has a meaning to propose a novel control structure based on IL made suitable for vehicle collision avoidance systems. The weakness of conventional IL was overcome by constructing a feedforward and feedback structure to make countless experiments involving the plant vehicle unnecessary and applying ID to ensure robustness to parameter changes. Real-time experiments verified the effectiveness of the proposed algorithm compared to existing IL methods, showing no issue applying the offline trained DNN in the simulation while showing robustness to parameter changes.

However, certain limitations were shown in this study, and future work can be done as follows. Firstly, this study does not consider the curvature of the road. An improved NMPC making the vehicle track the safety lane considering the road curvature should be developed. Secondly, the proposed method should be verified under various road frictions. Considering the road conditions, multiple pre-trained DNNs with different road frictions could be made and switched in the control structure. Thirdly, studies that verify the reliability of the DNN should be conducted to ensure more safety of the proposed IL-based control structure. Lastly, the proposed algorithm can be further compared with existing techniques that reduce the gap between the training and real-world domain, such as domain randomization.

Acknowledgments

This work was supported in part by the BK21+ FOUR Program of the National Research Foundation Korea (NRF) funded by the Ministry of Education (MOE), in part by Technology Innovation Program under Grant 20014983, Development of autonomous chassis platform for a modular vehicle funded by the Ministry of Trade, Industry & Energy (MOTIE, Korea), in part by NRF funded by the Korea Government (MSIP) under Grant 2020R1A2B5B01001531, in part by Autonomous Driving Technology Development Innovation Program funded by the MOTIE and Korea Evaluation Institute of Industrial Technology (KEIT), under Grant 20018181, Development of Lv. 4+ autonomous driving vehicle platform based on point-to-point driving to logistic center for heavy trucks, in part by NRF through Basic Science Research Program funded by MOE under Grant 2021R1A6A1A03043144, and in part by NRF funded by the Korean Government (MSIT) under Grant 2021R1C1C1003464.

References

[1] K. Bengler, K. Dietmayer, B. Farber, M. Maurer, C. Stiller, and H. Winner, "Three decades of driver assistance systems: Review and future perspectives," *IEEE Intelligent transportation systems magazine*, vol. 6, no. 4, pp. 6–22, 2014.

[2] Y. Hwang and S. B. Choi, "Adaptive collision avoidance using road friction information," *IEEE Transactions on Intelligent Transportation Systems*, vol. 20, no. 1, pp. 348–361, 2018.

[3] A. Ziebinski, R. Cupek, D. Grzechca, and L. Chruszczyk, "Review of advanced driver assistance systems (adas)," in *AIP Conference Proceedings*, vol. 1906, no. 1. AIP Publishing LLC, 2017, p. 120002.

[4] H. Lee and S. Choi, "Development of collision avoidance system in slippery road conditions," *IEEE Transactions on Intelligent Transportation Systems*, vol. 23, no. 10, pp. 19 544–19 556, 2022.

[5] J. Ji, A. Khajepour, W. W. Melek, and Y. Huang, "Path planning and tracking for vehicle collision avoidance based on model predictive control with multiconstraints," *IEEE Transactions on Vehicular Technology*, vol. 66, no. 2, pp. 952–964, 2016.

[6] Z. Zhu and H. Zhao, "Learning autonomous control policy for intersection navigation with pedestrian interaction," *IEEE Transactions on Intelligent Vehicles*, 2023.

[7] M. Everett, Y. F. Chen, and J. P. How, "Collision avoidance in pedestrian-rich environments with deep reinforcement learning," *IEEE Access*, vol. 9, pp. 10 357–10 377, 2021.

[8] J. Li, L. Yao, X. Xu, B. Cheng, and J. Ren, "Deep reinforcement learning for pedestrian collision avoidance and human-machine cooperative driving," *Information Sciences*, vol. 532, pp. 110–124, 2020.

[9] R. Hayashi, J. Isogai, P. Raksincharoensak, and M. Nagai, "Autonomous collision avoidance system by combined control of steering and braking using geometrically optimised vehicular trajectory," *Vehicle system dynamics*, vol. 50, no. sup1, pp. 151–168, 2012.

[10] M. Aripin, Y. Md Sam, K. A. Danapalasingam, K. Peng, N. Hamzah, and M. Ismail, "A review of active yaw control system for vehicle handling and stability enhancement," *International journal of vehicular technology*, vol. 2014, 2014.

[11] D. González, J. Pérez, V. Milanés, and F. Nashashibi, "A review of motion planning techniques for automated vehicles," *IEEE Transactions on intelligent transportation systems*, vol. 17, no. 4, pp. 1135–1145, 2015.

[12] N. H. Amer, H. Zamzuri, K. Hudha, and Z. A. Kadir, "Modelling and control strategies in path tracking control for autonomous ground vehicles: a review of state of the art and challenges," *Journal of intelligent & robotic systems*, vol. 86, pp. 225–254, 2017.

[13] K. Lee, S. Jeon, H. Kim, and D. Kum, "Optimal path tracking control of autonomous vehicle: Adaptive full-state linear quadratic gaussian (lqg) control," *IEEE Access*, vol. 7, pp. 109 120–109 133, 2019.

[14] R. Solea and U. Nunes, "Trajectory planning and sliding-mode control based trajectory-tracking for cybercars," *Integrated Computer-Aided Engineering*, vol. 14, no. 1, pp. 33–47, 2007.

[15] P. Petrov and F. Nashashibi, "Modeling and nonlinear adaptive control for autonomous vehicle overtaking," *IEEE Transactions on Intelligent Transportation Systems*, vol. 15, no. 4, pp. 1643–1656, 2014.

[16] C. Choi and Y. Kang, "Simultaneous braking and steering control method based on nonlinear model predictive control for emergency driving support," *International Journal of Control, Automation and Systems*, vol. 15, no. 1, pp. 345–353, 2017.

[17] C. Choi, Y. Kang, and S. Lee, "Emergency collision avoidance maneuver based on nonlinear model predictive control," in *2012 IEEE International Conference on Vehicular Electronics and Safety (ICVES 2012)*. IEEE, 2012, pp. 393–398.

[18] J. B. Rawlings, D. Q. Mayne, and M. Diehl, *Model predictive control: theory, computation, and design*. Nob Hill Publishing Madison, WI, 2017, vol. 2.
[19] K. Han, G. Park, G. S. Sankar, K. Nam, and S. B. Choi, "Model predictive control framework for improving vehicle cornering performance using handling characteristics," *IEEE Transactions on Intelligent Transportation Systems*, vol. 22, no. 5, pp. 3014–3024, 2020.
[20] B. Gutjahr, L. Gröll, and M. Werling, "Lateral vehicle trajectory optimization using constrained linear time-varying mpc," *IEEE Transactions on Intelligent Transportation Systems*, vol. 18, no. 6, pp. 1586–1595, 2016.
[21] A. Katriniok, J. P. Maschuw, F. Christen, L. Eckstein, and D. Abel, "Optimal vehicle dynamics control for combined longitudinal and lateral autonomous vehicle guidance," in *2013 European Control Conference (ECC)*. IEEE, 2013, pp. 974–979.
[22] J. Lee and S. B. Choi, "Integrated control of steering and braking for path tracking using multi-point linearized mpc," *IEEE Transactions on Intelligent Vehicles*, 2022.
[23] M. Brown and J. C. Gerdes, "Coordinating tire forces to avoid obstacles using nonlinear model predictive control," *IEEE Transactions on Intelligent Vehicles*, vol. 5, no. 1, pp. 21–31, 2019.
[24] J. Lee and S. Choi, "Nonlinear model predictive control for path tracking in high-speed corner entry situations," *International Journal of Automotive Technology*, vol. 23, no. 5, pp. 1373–1381, 2022.
[25] A. Hussein, M. M. Gaber, E. Elyan, and C. Jayne, "Imitation learning: A survey of learning methods," *ACM Computing Surveys (CSUR)*, vol. 50, no. 2, pp. 1–35, 2017.
[26] F. Torabi, G. Warnell, and P. Stone, "Behavioral cloning from observation," *arXiv preprint arXiv:1805.01954*, 2018.
[27] D. A. Pomerleau, "Alvinn: An autonomous land vehicle in a neural network," *Advances in neural information processing systems*, vol. 1, 1988.
[28] S. Ross, G. Gordon, and D. Bagnell, "A reduction of imitation learning and structured prediction to no-regret online learning," in *Proceedings of the fourteenth international conference on artificial intelligence and statistics*. JMLR Workshop and Conference Proceedings, 2011, pp. 627–635.
[29] A. Y. Ng, S. Russell *et al.*, "Algorithms for inverse reinforcement learning." in *Icml*, vol. 1, 2000, p. 2.
[30] J. Ho and S. Ermon, "Generative adversarial imitation learning," *Advances in neural information processing systems*, vol. 29, 2016.
[31] J. Carius, F. Farshidian, and M. Hutter, "Mpc-net: A first principles guided policy search," *IEEE Robotics and Automation Letters*, vol. 5, no. 2, pp. 2897–2904, 2020.
[32] T. Zhang, G. Kahn, S. Levine, and P. Abbeel, "Learning deep control policies for autonomous aerial vehicles with mpc-guided policy search," in *2016 IEEE international conference on robotics and automation (ICRA)*. IEEE, 2016, pp. 528–535.
[33] R. Wang, H. Li, and D. Xu, "Learning model predictive control law for nonlinear systems," in *2022 5th International Symposium on Autonomous Systems (ISAS)*. IEEE, 2022, pp. 1–6.
[34] T. Lee and Y. Kang, "Performance analysis of deep neural network controller for autonomous driving learning from a nonlinear model predictive control method," *Electronics*, vol. 10, no. 7, p. 767, 2021.
[35] T. Lee, D. Seo, J. Lee, and Y. Kang, "Real-time drift-driving control for an autonomous vehicle: Learning from nonlinear model predictive control via a deep neural network," *Electronics*, vol. 11, no. 17, p. 2651, 2022.
[36] R. Rajamani, *Vehicle dynamics and control*. Springer Science & Business Media, 2011.
[37] H. Pacejka, *Tire and vehicle dynamics*. Elsevier, 2005.
[38] T. Fujinaka and M. Araki, "Discrete-time optimal control of systems with unilateral time-delays," *Automatica*, vol. 23, no. 6, pp. 763–765, 1987.
[39] D. G. Zill, *Advanced engineering mathematics*. Jones & Bartlett Learning, 2020.
[40] P. T. Boggs and J. W. Tolle, "Sequential quadratic programming," *Acta numerica*, vol. 4, pp. 1–51, 1995.
[41] D. P. Kingma and J. Ba, "Adam: A method for stochastic optimization," *arXiv preprint arXiv:1412.6980*, 2014.
[42] A. Paszke, S. Gross, F. Massa, A. Lerer, J. Bradbury, G. Chanan, T. Killeen, Z. Lin, N. Gimelshein, L. Antiga *et al.*, "Pytorch: An imperative style, high-performance deep learning library," *Advances in neural information processing systems*, vol. 32, 2019.
[43] J. Snoek, H. Larochelle, and R. P. Adams, "Practical bayesian optimization of machine learning algorithms," *Advances in neural information processing systems*, vol. 25, 2012.
[44] H. Yin, P. Seiler, M. Jin, and M. Arcak, "Imitation learning with stability and safety guarantees," *IEEE Control Systems Letters*, vol. 6, pp. 409–414, 2021.
[45] X. He, "Building safe and stable dnn controllers using deep reinforcement learning and deep imitation learning," in *2022 IEEE 22nd International Conference on Software Quality, Reliability and Security (QRS)*. IEEE, 2022, pp. 775–784.
[46] "Simulink desktop real-time toolbox," https://www.mathworks.com/products/simulink-desktop-real-time.html, accessed: 2021-11-15.
[47] S. Hong, C. Lee, F. Borrelli, and J. K. Hedrick, "A novel approach for vehicle inertial parameter identification using a dual kalman filter," *IEEE Transactions on Intelligent Transportation Systems*, vol. 16, no. 1, pp. 151–161, 2014.
[48] K. Han, M. Choi, and S. B. Choi, "Estimation of the tire cornering stiffness as a road surface classification indicator using understeering characteristics," *IEEE Transactions on Vehicular Technology*, vol. 67, no. 8, pp. 6851–6860, 2018.
[49] J. Do, K. Han, and S. B. Choi, "Lane change–intention inference and trajectory prediction of surrounding vehicles on highways," *IEEE Transactions on Intelligent Vehicles*, 2023.
[50] A. Bajcsy, S. Bansal, E. Bronstein, V. Tolani, and C. J. Tomlin, "An efficient reachability-based framework for provably safe autonomous navigation in unknown environments," in *2019 IEEE 58th Conference on Decision and Control (CDC)*. IEEE, 2019, pp. 1758–1765.

Seungtaek Kim received a B.S. degree in Mechanical Engineering from Yonsei University, Seoul, Korea, and an M.S. in Mechanical Engineering from Korea Advanced Institute of Science and Technology (KAIST), Daejeon, Korea, in 2019 and 2021, respectively. Since 2021, he is currently pursuing the Ph.D. in Mechanical Engineering at KAIST. His research interests include vehicle dynamics and control, path tracking, and advanced driving assistant systems.

Kyoungseok Han received a B.S. degree in Civil Engineering (minor in Mechanical Engineering) from Hanyang University, Seoul, Korea, in 2013, and the M.S. and Ph.D. degrees in Mechanical Engineering from the Korea Advanced Institute of Science and Technology (KAIST), Daejeon, Korea, in 2015 and 2018, respectively. He was a Research Fellow at the University of Michigan from June 2018 to February 2020. In March 2020, he was appointed Assistant Professor at the School of Mechanical Engineering, Kyungpook National University. His research interests include vehicle dynamics and control, autonomous vehicles, battery electric vehicles, optimization, and control theory.

Seibum B. Choi received a B.S. in Mechanical Engineering from Seoul National University, Seoul, Korea, an M.S. in Mechanical Engineering from KAIST, Daejeon, Korea, and a Ph.D. in control from the University of California, Berkeley, CA, USA, in 1993. From 1993 to 1997, he was involved in developing automated vehicle control systems at the Institute of Transportation Studies, University of California. Through 2006, he was with TRW, Livonia, MI, USA, where he was involved in developing advanced vehicle control systems. Since 2006, he has been faculty in the Mechanical Engineering Department of KAIST, Korea. His research interests include fuel-saving technology, vehicle dynamics and control, and active safety systems. Prof. Choi is a Member of the American Society of Mechanical Engineers, the Society of Automotive Engineers, and the Korean Society of Automotive Engineers.